A&A 545, A59 (2012)
DOI: 10.1051/0004-6361/201219234

Astronomy & Astrophysics

The relationship between γ Cassiopeiae's X-ray emission and its circumstellar environment

II. Geometry and kinematics of the disk from MIRC and VEGA instruments on the CHARA Array

Ph. Stee[1], O. Delaa[1], J. D. Monnier[3], A. Meilland[1], K. Perraut[2], D. Mourard[1], X. Che[3], G. H. Schaefer[8], E. Pedretti[14], M. A. Smith[4], R. Lopes de Oliveira[5], C. Motch[6], G. W. Henry[7], N. D. Richardson[8], K. S. Bjorkman[9], R. Bücke[10], E. Pollmann[11], J. Zorec[13], D. R. Gies[8], T. ten Brummelaar[8], H. A. McAlister[8], N. H. Turner[8], J. Sturmann[8], L. Sturmann[8], and S. T. Ridgway[12]

[1] Laboratoire Lagrange, UMR 7293 UNS-CNRS-OCA, Boulevard de l'Observatoire, BP 4229, 06304 Nice Cedex 4, France
e-mail: Philippe.Stee@oca.eu
[2] UJF-Grenoble 1/CNRS-INSU, Institut de Planétologie et d'Astrophysique de Grenoble (IPAG) UMR 5274, 38041 Grenoble, France
[3] Department of Astronomy, University of Michigan, Ann Arbor, MI 48109, USA
[4] Catholic University of America, 3700 San Martin Dr., Baltimore, MD 21218, USA
[5] Universidade Federal de Sergipe, Departamento de Física, Av. Marechal Rondon s/n, 49100-000 São Cristóvão, SE, Brazil
[6] Université de Strasbourg, CNRS, Observatoire Astronomique, 11 rue de l'Université, 67000 Strasbourg, France
[7] Center of Excellence in Information Systems, Tennessee State University, 3500 John A. Merritt Blvd., Box 9501, Nashville, TN 37209, USA
[8] Center for High Angular Resolution Astronomy, Department of Physics & Astronomy, Georgia State University, PO Box 4106, Atlanta, GA 30202-4106, USA
[9] Ritter Astrophysical Research Center, Department of Physics & Astronomy, University of Toledo, 2801 W. Bancroft, Toledo, OH 43606, USA
[10] Anna-von-Gierke-Ring 147, 21035 Hamburg, Germany
[11] Emil-Nolde-Str. 12, 51375 Leverkusen, Germany
[12] National Optical Astronomical Observatory, 950 North Cherry Ave., Tucson, AZ 85719, USA
[13] UPMC Univ. Paris 06, UMR 7095, Institut d'Astrophysique de Paris, 98bis Bd. Arago, 75014 Paris, France
[14] School of Physics and Astronomy, University of St Andrews, North Haugh, St Andrews, Fife, KY16 9SS, UK

Received 16 March 2012 / Accepted 1 August 2012

ABSTRACT

Context. γ Cas is thought to be the prototype of classical Be stars and is the most studied object among this group. However, as for all Be stars, the origin and the physics of its circumstellar disk responsible for the observed near IR-excess, emission lines, and peculiar X-ray emission is still being debated.
Aims. We constrain the geometry and kinematics of its circumstellar disk from the highest spatial resolution ever achieved on this star. This investigation is a part of a large multi-technique observing campaign to obtain the most complete picture of γ Cas which emphasizes the relation of the circumstellar environment to the star's X-ray flux.
Methods. We present new observations in the near infrared (MIRC) and in the visible (VEGA) obtained with the CHARA interferometer. The VEGA instrument allows us to not only obtain a global disk geometry but also spectrally dispersed visibility modulus and phases within the Hα emission line, which enables us to study the kinematics within γ Cas's disk.
Results. We obtain a disk extension in the nearby Hα continuum of 1.72 stellar diameter and 1.86 stellar diameter in the H band at 1.65 μm assuming a Gaussian disk model but also compatible with an elliptical ring model with a minor internal diameter of 1.38 stellar diameter in H. For the first time we demonstrate that the rotation mapped by the emission in the Hα line within the disk of γ Cas and up to 10 $R_\star$ is Keplerian.
Conclusions. These observations have pushed the size of the disk to greater proportions. γ Cas was also confirmed to be a nearly critical rotator. The disk imaging gives neither indication of a 1-arm spiral feature nor evidence of a secondary star reinforcing the interpretation that the secondary is certainly a low-mass and low-luminosity star or a degenerate companion.

Key words. techniques: interferometric – stars: emission-line, Be – stars: winds, outflows – circumstellar matter – binaries: close

1. Introduction

The "Be phenomenon" is defined as B type, non-supergiant stars that have at least once exhibited Balmer lines in emission with an infrared excess produced by free-free and free-bound processes in an extended circumstellar disk. Be stars as a group are also rapid rotators and often show variability in UV/optical/IR wavelengths on a variety of timescales. There is now strong evidence that the disk around Be stars is close to Keplerian (Meilland et al. 2011b) and that this equatorial disk is slowly expanding, e.g. $V_r \sim 1$ km s^{-1} (Miroshnichenko et al. 2003; Kanaan et al. 2008).

However, a few key issues remain unsolved on the actual structure of the circumstellar envelopes around Be stars. These include identifying the dominant mass ejection mechanism from the central star and determining how matter is redistributed in the star's immediate environment. These issues cannot be resolved by using a single telescope or a single observing technique. However, because Be disks can extend up to a few milliarcseconds (mas) for the closest Be stars, instrumental technology has evolved to the point where long baseline optical interferometry (LBOI) permits the combination of high spatial and spectral resolution. In fact, is now arguably the most suitable technique to probe the circumstellar environments of Be stars, thereby bringing new insights into the physics of Be stars.

Nevertheless, even if much progress has been made, the basic physical processes that produce the "Be phenomenon" from a B classical star are still not yet understood. The high rotational rates of Be stars seems to be a primary condition leading to the production of Be decretion disks, as proposed by Struve (1931) 80 years ago, particularly if most of them are rotating close to their critical velocity.

The fast rotation of active hot stars also causes the stellar disk to become oblate. Another physical effect is the gravity darkening or the von Zeipel effect (von Zeipel 1924) which causes the surface gravity and the emitted flux to decrease from the poles to the equator. This effect was directly measured by Domiciano de Souza et al. (2003) with the VLTI for the Be star α Eri (Achernar). Their measurements correspond to a major/minor axis ratio of 1.56 ± 0.05, i.e., an extreme oblateness that rules out the commonly adopted Roche approximation in which the rotation is supposed to be uniform and the mass centrally condensed. This might also be the evidence that some Be stars are rotating close to their critical velocities. Achernar oblateness was measured again by Carciofi et al. (2008) and found a slightly smaller ratio of ~1.4–1.5 depending on the adopted stellar rotation rate.

Thus, the study of the physics of Be stars, and particularly of the Be prototype γ Cas (=27 Cas, HR 264, HD 5394, HIP 4427, MWC 9, ADS 782A), is an exciting field. 145 years after the discovery of its emission lines by Padre Secchi (1867) γ Cas has not completely delivered all its secrets. This star is more or less a Pandora's box where each new finding opens many new questions. It is clear that the resolution of the interaction of the star and its disk entails knowledge that will combine several fields in stellar physics, including the evolution of massive stars, interacting binaries, magnetic field evolution, asteroseismology, formation of stellar winds and mass loss. More details can be found in the review by Porter & Rivinus (2003) which highlights many results on Be stars and links to general astrophysics.

In a series of papers we present a combined multidisciplinary effort to understand the relationship between the star's high energy emission, its intrinsic parameters, its binarity, and its interaction with its surrounding "decretion" disk. The first paper of the series, Smith et al. (2012, hereafter "Paper I") emphasized the relationship between the physical description of X-ray emitting sites, which must be both complex and numerous, and its circumstellar environment. We put this study in the context of contemporaneous optical visible-band photometry, variability in its Hα and He I λ6678 lines as well as an updated description of its binary orbit around a secondary of unknown type.

In this interferometric campaign, we present recent and original interferometric CHARA/MIRC and CHARA/VEGA observations of γ Cas to see how the multidisciplinary study can lead us to an understanding of the "γ Cas variability phenomenon".

For the last several decades γ Cas has been discontinuously feeding matter to its decretion disk and many of the variations of optical and X-ray flux of γ Cas are likely to be due to matter released by the Be star or its interactions with previously released matter. In this paper, we would like to address the following points:

- If there is a strong coupling between a putative magnetic field and the circumstellar disk which may lead to part of the observed X-ray emission, is the disk forced to rotate as a solid body by the magnetic field? What are the kinematics within γ Cas's circumstellar environment?
- Following the classical picture of magnetic interaction for T Tauri stars and their associated disks, a stellar corotating magnetosphere may be present leading to a gap between the stellar surface and the inner part of the disk. Is there any evidence of such a "ring" in our interferometric data? Is the disk in contact with the central star?
- Is there still any proof for a disk asymmetry already measured as a 1-armed density structure by Berio et al. (1999) in Hα more than a decade ago?
- If γ Cas is feeding matter to its decretion disk, did the extension of the disk increase its size during this last decade?
- Since the binarity of γ Cas is now well established, (see for instance Harmanec et al. 2000; Nemravová et al. 2012), do we have any evidence for a companion in our interferometric data?

The paper is organized as follows. In Sect. 2 we summarize the X-ray properties obtained from Paper I. Section 3 outlines the history of γ Cas interferometric observations. In Sect. 4 we present the CHARA observations and the data reduction process with the VEGA and MIRC instruments. A first analysis using geometrical models is presented in Sects. 4 and 5 and more advanced interpretation of the differential data using a kinematic model is presented in Sect. 6. Finally, we discuss our results in Sect. 7 and draw conclusions in Sect. 8.

2. The X-ray properties

X-ray flux was first reported in the direction of γ Cas by Jernigan (1976). However, γ Cas actually garnered attention as an interesting X-ray object following the *Einstein* observations of White et al. (1982). Since this work the star has been observed by almost every major astronomical X-ray satellite. It is now understood to be the prototype of several such Galactic objects. All are B0.5-1.5e III-V stars with rotationally broadened spectral lines (Motch et al. 2007). The X-ray characteristics of these objects are among the most peculiar of any X-ray emitting massive stars (Güdel & Nazé 2009).

The X-ray emissions of these objects exhibit moderate luminosities ($L_x \sim 3$–10×10^{32} erg s^{-1}). The spectra are dominated by a hot ($kT \sim 14$ keV) optically thin thermal component and have 2–3 "warm/cold" secondary components. They also exhibit a Fe K fluorescence feature at 1.9 Å, indicating proximity to cold gas. γ Cas's X-ray light curve exhibits ubiquitous rapid flaring (Smith et al. 1998) and long cycles of 50–91 days (Robinson et al. 2002). An analysis of the energetics of flares indicates that they must be emitted in a high density ($\geq 10^{14}$ cm^{-3}) environment (Smith et al. 1998). The long cycles may be associated with long cycles observed at optical wavelengths (Robinson et al. 2002). Some peculiar results determined from γ Cas spectra include anomalies in the abundances of Fe, N, and Ne, and Paper I showed that these may be time-dependent. Significantly, this paper also found that one of two column densities needed to model the soft X-ray continuum is highly time dependent.

The mechanism responsible for the hard thermal X-ray emission in γ Cas analogs has been a matter of conjecture, and two quite different explanations have been advanced. These are accretion onto a compact object (e.g., a white dwarf) and magnetic ejection of material at the Be star-disk interface. Advocates of the accretion scenario point to the general success of explaining X-ray emissions from Be systems in close binaries, the rough similarity to X-ray plasma conditions found from models of X-ray spectra of CV systems, and the otherwise inability to identify degenerate companions in Be stars owing to their relative faintness. Advocates of the magnetic star-disk picture point to (for the most part) simultaneous correlations of rapid X-ray fluxes with variations in UV light and spectral line fluxes that can only be associated with an early type main sequence B star. These multiband correlations were summarized in Paper I and refer to work of Robinson et al. (2002), Smith & Robinson (1999), Robinson & Smith (2000), and Smith & Robinson (2003).

A (weakly) magnetic disk already appears to be implicated somehow in the X-ray generation process because it appears to be the place in which both optical and X-ray "long cycles" originate (Smith et al. 2006; Henry & Smith 2012). This suggests the presence of disk oscillations such as from a magnetic dynamo. The interaction between field lines associated with matter constrained by solid body rotation above the star and field lines in the Keplerian disk would lead to a stretching, severing, reconnection, and relaxation of field lines. These events would accelerate high energy electron beams, some of them toward the Be star. In this scenario the impact of these beams on its surface would produce localized expanding hot plasma parcels, which emit copious hard X-rays (see also Robinson & Smith 2000).

Paper I supported to the latter argument by showing that the one of the two X-ray-derived column densities is well correlated with optical brightening and reddening in the disk. Therefore, the source of the hard X-rays must lie beyond this absorption column relative to the observer. The Paper I authors attributed this column to efflux from the Be star. It is now clear that the X-ray plasma conditions are somehow tied to the growth of the Be decretion disk. In this paper we will report a (negative) search for disk asymmetries that would identify the source of this column.

3. 25 years of interferometry on γ Cas

The first interferometric measurements of γ Cas were obtained by Thom et al. (1986) in the continuum and in the Hα emission line using the I2T interferometer. The authors derived a 3.25 mas diameter for the circumstellar environment in Hα.

Later, Mourard et al. (1989) used the sensitivity of the GI2T inteferometer to combine for the first time high spatial resolution and medium spectral resolution to show that the envelope around γ Cas was in motion compatible with Keplerian rotation and was approximately fit with a disk model.

Quirrenbach et al. (1993) exploited the capability of the MkIII interferometer to cover a large (u, v) plane and definitively proved that the γ Cas envelope was not spherical but rather elongated and oriented 20° east with respect to the north-south direction. They also derived an inclination angle of at least 42°. These results confirm the usual picture for the origin of the linear polarization by electron scattering in a flattened environment. Using the same instrument, Quirrenbach et al. (1997) obtained an extension of 3.47 mas for the γ Cas circumstellar disk in a narrow band filter centered on Hα.

Stee et al. (1995) presented a radiative wind model of γ Cas based on spectroscopic and interferometric data collected with the GI2T. They found that 90% of the Hα emission originates from an ellipsoid with an axis ratio of 0.72. The major axis was about 8.5 stellar diameters, which corresponds to about 4 mas assuming a stellar diameter of 0.44 mas for the stellar photosphere.

In 1997, Rousselet-Perraut et al. (1997) reported an attempt to detect polarization effects in the envelope of γ Cas with the GI2T. They obtained an upper limit of 1.3 on the ratio of the angular diameters of the envelope seen through polarizers parallel and perpendicular to the north-south direction of the GI2T's baseline. Assuming that the continuum flux originates within a photosphere surrounded by an elliptical Gaussian envelope they estimated its extent to 2.9 ± 0.5 mas in Hα.

Stee et al. (1998) reported the first spectrally resolved observations with the GI2T of γ Cas in the He I λ6678 and Hβ emission lines. Putting all these different measurements together, they found that the envelope size in the visible increases following the sequence: He I λ6678 (2.3 R_*), 0.48 μm continuum (2.8 R_*), 0.65 μm continuum (3.5 R_*), Hβ ($\lesssim$8.5 R_*), and Hα (18 R_*). Using these measurements, Stee (2003) predicted for γ Cas a disk opening angle of 54° and a mass of the disk of about 4.3×10^{-9} $M_\odot$.

From interferometric observations over several years Berio et al. (1999) discovered a prograde rotation (that is, in the sense of the disk's rotation) of a one-armed density pattern in the disk of γ Cas. This prograde precession agrees with Okazaki's (1997) model of a one-armed ($m = 1$) oscillation confined by radiative effects. In their paper, Berio et al. (1999) have investigated how such oscillations occur within the equatorial regions of the latitude-dependent radiative wind model developed by Stee & Araújo (1994). In this model the star is distorted due to its fast rotation. The centrifugal force causes the effective gravity and the brightness temperature to decrease from pole to equator, and thus the corresponding radiative force will depend on the stellar latitude. Finally, the star has a highly ionized fast wind in the polar regions and a slow wind of low ionization, with a higher density near the equator. In the inner ($\leq$10 R_*), cool, dense equatorial regions, the kinematics are dominated by the Keplerian rotation, while the one-armed oscillations develop in the radiative wind driven by optically thin lines.

γ Cas was observed with NPOI by Tycner et al. (2003). Their best fit of an elliptical Gaussian model in Hα has an average angular size of the major axis of 3.67 ± 0.09 mas, an average axial ratio of 0.79 ± 0.03 and an average PA of $32° \pm 5°$ all in good agreement with values reported previously in this paper.

In 2006 Grundstrom & Gies (2006) demonstrated that there is a monotonic relationship between the emission-line equivalent width and the ratio of the angular half-width at half-maximum of the projected disk major axis to the radius of the star. γ Cas measurements at different times show a similar monotonic relationship.

Using the NPOI interferometer, Tycner et al. (2006) obtained the highest spatial resolution measurements of the Hα-emitting regions of γ Cas to date. They demonstrated that the intensity distribution in the circumstellar region cannot be represented by uniform disk or ringlike structures, whereas a Gaussian intensity distribution appears to be fully consistent with their observations. They obtain an upper limit for the full opening angle for γ Cas of 34°, which is significantly less than the 54° obtained by Stee (2003).

Finally, Gies et al. (2007) presented the first K'-band observations of γ Cas with the CHARA Array Interferometer. They found that the angular size of the K' disk emission is smaller than that determined for the Hα emission, and they argued that

the difference is the result of a larger Hα opacity and the relatively larger neutral hydrogen fraction with increasing radial distance from the star. They found that the Hα emission is more extended along the major axis and that the half maximum intensity radii are located at 2.6 and 7.4 $R_\star$ for the K'-band and Hα intensities respectively.

4. CHARA observations of γ Cas

Following the previous studies, we have conducted a multi-technique, multi-site observing campaign, including Automated Photometric Telescopes (APT) measurements, *XMM-Newton* observations, Hα spectroscopic follow-up from the Ritter Observatory and Long Baseline Optical Interferometry in the near infrared (MIRC) and in the visible (VEGA) with the CHARA interferometer. We report in the following the results from the interferometric campaign whereas other multi-technique, multi-site observations are reported in Paper I. Note that compared to previous interferometric data reported in Sect. 3 our new CHARA/VEGA and CHARA/MIRC observations presented below are more sensitive than GI2T measurements (see Mourard et al. 2009), and are providing a larger angular resolution and a better (u, v) plane coverage than previous observations.

4.1. VEGA data

4.1.1. Observations

The VEGA instrument (Mourard et al. 2009) operating at the CHARA array located on the Mount Wilson Observatory (LA, California, USA), operates in the visible domain and benefits from a spectrograph and a polarimeter. The spectrograph is designed to sample the visible band from 0.45 to 0.85 μm (hereafter R band). It is equipped with two photon counting detectors observing at two different spectral bands.

The simultaneous operation of the two detectors is only possible in high and medium spectral resolution. The optical design allows simultaneous recording of the data, in medium spectral resolution, of the spectral region around Hα on the red detector and around Hβ on the blue detector. Observing in the blue requires excellent seeing, which was not the case during our observing runs, and thus, we only have usable data from the red camera. The medium (5000) and high (30 000) spectral resolutions are well suited to perform kinematic analysis of the interferometric signal, providing a velocity resolution of 60 and 10 km s^{-1} respectively.

The polarimeter is composed of a Wollaston prism to separate two orthogonal polarization states and a movable quarter wave plate. A fixed quarter wave plate is placed after the Wollaston prism to transform the two linearly polarized output beams into two circularly polarized beams. This helps avoid unbalanced transmission by the grating. After being spectrally dispersed, the two beams carrying both the interference pattern and the polarization information are focused on the photon-counting detectors that contain two (x, λ) images, one per polarization state referred to as High and Low with respect to their position on the detector. As previously detailed (Rousselet-Perraut et al. 2006), such a device can measure three (I, Q, and V) of the four Stokes parameters.

γ Cas CHARA/VEGA observations were carried out between 2008 October and 2010 August with the Red detector centered around 6562 Å. The spectrograph resolution used was medium ($R \sim 5000$) and high ($R \sim 30\,000$) and some observations in polarimetric mode were recorded (Table 1). Most observations used two of the six one-meter telescopes which compose the CHARA Array but also some with a triplet of telescopes (E1E2W2), leading to the (u, v) coverage displayed in Fig. 1-right.

We have also recorded polarimetric data with the Wollaston prism only. We recorded fringe patterns in linearly polarized light (with the Wollaston prism inserted in the VEGA beam) interleaved with fringe patterns in natural light (when the Wollaston prism is removed). We have made measurements on γ Cas and on its calibrator HD 6961 on 2010 July 31 and August 1 (see last rows of Table 1).

4.1.2. Data reduction

The Hα spectrum (Fig. 2) and differential visibility modulus and phase (see Sect. 5) were estimated using cross-spectral analysis with parameters in Table 1. Hα spectra taken from the BeSS database[1] are overplotted in Fig. 2. These line profiles were recorded 2008 September 26 and October 9. The Hα VEGA/CHARA line profile (in blue in Fig. 2) was recorded 2008 October 8. Hence, line profiles from spectra obtained by amateur astronomers have been chosen as close as possible to the epoch of our observations – it is expected be similar to its interferometric counterpart, both in terms of global intensity and in morphology when reduced to the same spectral resolution. As already outlined in Delaa et al. (2011), the VEGA/CHARA red detector underestimates the line flux by a factor 1.5–2. This is probably due to a saturation phenomenon that correlates with the brightness of the object, but not with the line intensity. Hence, it is not a local effect that concerns the detector, but only the photon counting algorithm. Accordingly, the measured visibilities and phase signals are not significantly affected by this phenomenon, as already tested and discussed in Delaa et al. (2011).

The data reduction used the software developed by the VEGA group and described in Mourard et al. (2009). This software offers two data reduction modes:

- In the spectral density mode, we obtain one measurement, i.e. the squared visibility averaged on a spectral band centered at a given wavelength λ.
- With the cross-spectral analysis mode, we obtain the visibility modulus $V(\lambda)$ and the differential phase $\phi_{\rm diff}(\lambda)$ within a narrow channel having a few Angstroms width, which is translated, step by step, across a large reference spectral band. For each step, we measure the product $V(\lambda1)\times V(\lambda2)$ and $\phi_{\rm diff}(\lambda2)$.

The raw visibilities in the continuum for γ Cas and its calibrators were estimated in the spectral density mode using pass-band parameters in Table 1. To calibrate the data the angular limb-darkened diameters of the calibrators $\theta_{\rm LD}$ were estimated using the SearchCal software (Bonneau et al. 2006) from the Jean-Marie Mariotti Center[2]. We adopt $\theta_{\rm LD} = 0.48 \pm 0.03$ mas for HD 6961, $\theta_{\rm LD} = 0.307 \pm 0.021$ mas for HD 3360, and $\theta_{\rm LD} = 0.287 \pm 0.014$ mas for HD 12303.

The polarimetric data were processed by cross-spectral analysis with the same parameters for the natural and the polarized observations. Since the calibrator is much fainter than the target, the signal-to-noise ratio was not enough to reach the same spectral resolution on the differential observables of γ Cas and of its

[1] http://basebe.obspm.fr
[2] http://www.jmmc.fr/searchcal/

Table 1. VEGA/CHARA observing logs and parameters for the auto-correlation and cross-correlation data reduction processes.

Observing date		Tel.	Proj. baseline L (m)	PA (deg)	r_0 (cm)	$\lambda/\Delta\lambda$	Pol.	Calib. (HD)	Auto-corr. (continuum) λ_0 (nm)	$\delta\lambda$ (nm)	$V^2_{\rm cont}$ (nm)	Cross-corr. (Hα) $\delta\lambda_{\rm cross}$ (nm)	$\Delta\lambda_{\rm cross}$ (nm)
2008 Oct. 08	08.27	S1-S2	29.8	−19	15	5000	none	6961	646.1	12.5	0.87 ± 0.05	0.4	20
									664.1	9	0.86 ± 0.06		
	08.42	S1-S2	29.7	−21	15	5000	none	6961	646.1	12.5	0.85 ± 0.05	0.4	20
	08.55	S1-S2	29.5	−23	15	5000	none	6961	646.1	12.5	0.88 ± 0.06	0.4	20
									664.1	9	0.88 ± 0.10		
2009 Jul. 25	11.51	W1-W2	107.4	109.1	9	5000	none	3360	669.0	18	0.50 ± 0.02	–	–
2009 Jul. 31	12.03	W1-W2	107.9	100.1	20	5000	none	3360	669.0	18	0.43 ± 0.02	–	–
2009 Aug. 01	10.12	W1-W2	105.4	122.8	10	5000	none	3360	669.0	18	0.54 ± 0.02	–	–
2009 Oct. 26	07.13	S1-S2	29.8	−20	6	5000	none	12303	669.5	17	0.63 ± 0.04	–	–
2009 Nov. 17	02.14	S1-S2	30.2	13.8	15	30 000	none	none	–	–	–	0.05	5.5
	02.33	S1-S2	30.3	11.7	12	30 000	none	none	–	–	–	0.05	5.5
	02.45	S1-S2	30.4	9.7	15	30 000	none	none	–	–	–	0.05	5.5
2009 Nov. 18	04.17	S1-S2	30.0	−5.8	12	30 000	none	none	–	–	–	0.05	5.5
2009 Nov. 20	04.15	W1-W2	107.5	107.2	10	5000	none	3360	669.5	17	0.51 ± 0.04	–	–
2010 Jul. 29	11.02	W1-W2	106.4	116.5	10	5000	none	3360	672.8	21	0.50 ± 0.03	0.4	20
	11.26	W1-W2	107.5	111.13	10	5000	none	3360	672.8	21	0.50 ± 0.03	0.4	20
	11.48	W1-W2	107.6	106.8	10	5000	none	3360	672.8	21	0.50 ± 0.02	0.4	20
2010 Jul. 30	07.32	W1-W2	98.0	169.2	11	5000	none	3360	672.5	21	0.44 ± 0.01	–	–
	10.17	W1-W2	104.73	126.5	10	5000	none	3360	672.5	21	0.47 ± 0.02	0.4	20
2010 Jul. 31	08.52	S1-S2	29.8	19.4	8	5000	none	6961	669.25	16.5	0.91 ± 0.03	0.4	20
	09.04	S1-S2	30.0	17.4	8	5000	Woll.	6961	–	–	–	0.4	20
	09.25	S1-S2	30.1	14.7	9	5000	none	6961	669.25	16.5	0.88 ± 0.03	0.4	20
2010 Aug. 01	10.01	S1-S2	30.4	7.9	10	5000	none	6961	669.75	17.5	0.82 ± 0.02	0.4	20
	10.32	S1-S2	31.8	3.6	10	5000	Woll.	6961	–	–	–	0.4	20
	11.03	S1-S2	30.5	−2.5	10	5000	none	6961	669.75	17.5	0.77 ± 0.02	0.4	20
2010 Aug. 29	10.57	E2-E1	65.5	−133.7	??	5000	none	3360	672.00	20	$6.4 \pm 0.6 \times 10^{-2}$	–	–
		E2-W2	155.8	−127.1							$2.1 \pm 0.1 \times 10^{-2}$	–	–
		E1-W2	221.0	−129.1							$9.6 \pm 2.7 \times 10^{-3}$	–	–
2010 Aug. 29	11.37	E2-E1	65.8	−143.3	??	5000	none	3360	672.00	20	$7.0 \pm 0.2 \times 10^{-2}$	–	–
		E2-W2	156.2	−136.8							$1.8 \pm 0.1 \times 10^{-2}$	–	–
		E1-W2	221.8	−138.8							$2.9 \pm 2.0 \times 10^{-3}$	–	–

calibrator. To avoid increasing the error bars in our result from the calibration procedures, we computed only the differential observables across the Hα line with the cross-spectral analysis and then adjusted the continuum visibility level by means of the visibility squared determination in the continuum (see last columns of Table 1). We verified from the calibrator processed data that no differential effect is present between the natural and the polarized observations. From this CHARA baseline (S1S2) no instrumental polarization affects our data beyond our error bars, as previously confirmed from the squared visibility measurements of different sources by Mourard et al. (2009).

4.2. MIRC data

4.2.1. Observations

The Michigan Infrared Combiner (MIRC) was used at the CHARA Array to obtain multiple baseline and closure phase information for γ Cas. At the time of these observations, MIRC combined four of the six CHARA telescopes simultaneously, resulting in measurements of 6 squared-visibilities and 4 closure phases at a time. By changing the telescopes used with MIRC, one can obtain excellent Fourier coverage within a few nights. MIRC was used in H band ($\lambda_0 = 1.65\ \mu$m) mode using a prism that split the light into 8 spectral channels ($\frac{\lambda}{\Delta\lambda} \sim 40$). These observations benefitted from the recent upgrade to include "photometric channels" (Che et al. 2010), resulting in improved calibration of visibility amplitudes. More information on the MIRC instrument can be found in Monnier et al. (2004) and Monnier et al. (2006).

Here we present results from 5 nights of MIRC observations that were planned to roughly coincide with contemporaneous X-ray observations presented in Paper I. Table 2 lists the relevant observing information, including the calibrators and their adopted angular diameters. The UV coverage for these nights can be found in Fig. 1 (left panel).

4.2.2. Data reduction

The data reduction procedure for MIRC has been described in a number of recent papers (Monnier et al. 2007; Che et al. 2011; Zhao et al. 2011). The basic idea is to average the power spectrum of the fringe pattern for each baseline in each spectral channel and to apply a bias correction to account for photon and read noise. We adopted a coherent integration time of 17 ms, short enough to essentially freeze the atmosphere and maintain good calibration against changes in temporal coherence. The closure phases were measured by averaging the bispectrum consisting

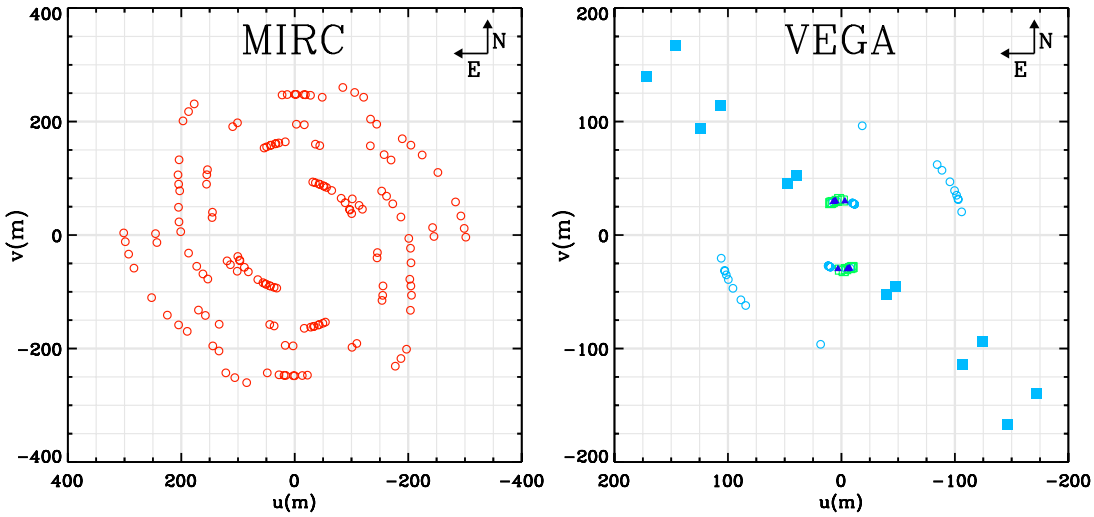

Fig. 1. *Left.* MIRC/CHARA (u, v) plane coverage of γ Cas. *Right.* VEGA/CHARA (u, v) plane coverage of γ Cas. Blue open circles = 2T MR data, dark blue triangles: 2T HR data, blue square: 3T MR data and green rectangle: 2T polarimetric data.

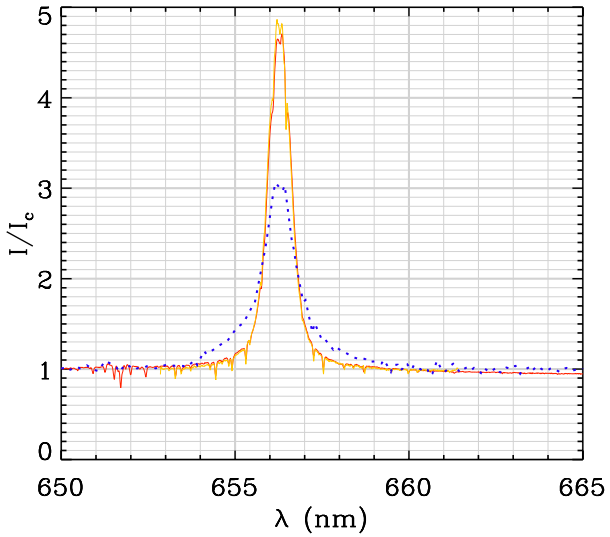

Fig. 2. Medium spectral resolution Hα CHARA/VEGA line profiles (blue dotted line) of γ Cas, recorded 2008 October 8. Red and yellow solid lines are amateur spectra obtained from the BeSS database, recorded on 2008 September 26 and October, 9.

of all sets of closed triangles. We monitored the instrumental transfer function by observing calibrator stars with angular sizes estimated through surface brightness relations. Before fitting models to our data, we averaged the squared-visibility and bispectral data into blocks of about 10 min and increased the error bars to account for residual systematics ($\Delta V^2 > 0.0002$, $\frac{\Delta V^2}{V^2} > 0.05$, $\Delta\Phi_{CP} > 0.5°$). The full dataset is available in OI-FITS format (Pauls et al. 2005) upon request.

5. Disk geometry in the visible and near-IR continuum

5.1. The LITPRO software

To model the continuum visibility modulus and closure phases obtained from our MIRC and VEGA observations we used the LITpro[3] model fitting software for optical/infrared interferometric data developed by the Jean-Marie Mariotti Center (JMMC) to analyze our data (Tallon et al. 2008). It is based on the Levenberg-Marquardt algorithm, which allows a fit to converge to the closest χ^2 local minimum from a set of initial values of the model parameters. It also includes tools for facilitating the search for the global minimum. LITpro calculates an error on the fitted parameters based on the χ^2 value at the minimum. It uses data error estimates based on the OI FITS format, which does not include error correlation estimates. Therefore, in some cases, LITpro can provide underestimated errors on the parameters.

5.2. The models

To test the possibility of the presence of a cavity between the stellar surface and the circumstellar disk we analyzed our datasets using two different models:

1. A central star modeled as uniform disk with a 0.44 mas extension + an extended elliptical Gaussian distribution + a background emission. This model has then four free-parameters: the FWHM of the major axis of the Gaussian distribution ($\theta_{\rm disk}$); the relative environment continuum flux ($F_{\rm disk}$), the flattening ratio of the major to the minor Gaussian distribution axis (f), and the position angle of the major axis of the disk measured eastward from the north (PA).
2. The same central star + a flattened ring + a background emission. This model has 6 free-parameters: the disk inner-rim diameter ($\theta_{\rm disk}$), the ring width ($\delta\theta_{\rm disk}$), the relative ring flux ($F_{\rm disk}$), the relative background flux ($F_{\rm bg}$), the flattening ratio (f), and the major-axis position angle (PA). The motivation for this ring model was to determine whether there is a star-disk gap that might arise from solid body rotation of clouds within the radius, as proposed in Paper I to interpret the observed X-ray emission.

5.3. Results

The best-fit parameters from the Visible and near-IR band models are presented in Table 3 and the corresponding intensity

[3] LITpro software available at http://www.jmmc.fr/litpro

Table 2. MIRC/CHARA observing log.

UT date	Configuration	Calibrator(s) (UD diameter)
2010 Aug. 05	S2-E1-W1-W2	7 And (0.66 ± 0.02 mas), 37 And(0.68 ± 0.02 mas)
2010 Aug. 08	E1-W2-W1-W2	37 And
2010 Sep. 24	S2-E2-W1-W2	7 And, θ Cas (0.57 ± 0.04 mas)
2010 Nov. 04	S1-E2-W1-W2	7 And, 36 Per (0.51 ± 0.03 mas)
2010 Nov. 05	S1-E1-W1-W2	7 And, 36 Per

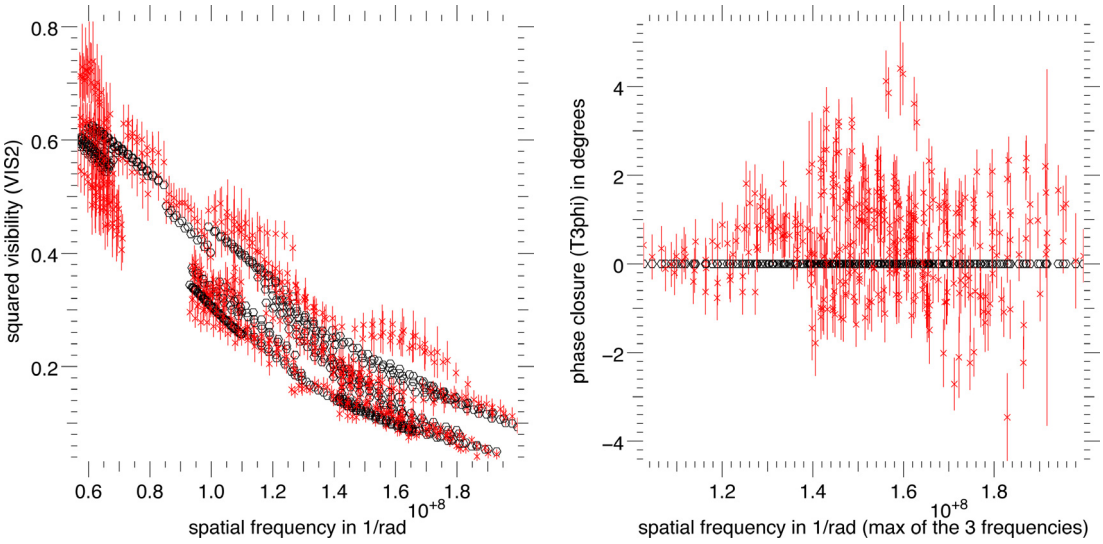

Fig. 3. MIRC visibilities (*left*) and closure phases (*right*) observed (red crosses) and modeled (black circles) as a function of spatial frequency points where data were taken.

distributions are plotted in Fig. 4. Although our CHARA data does not have the angular resolution to constrain directly the oblateness of the central star, we have used the estimation of the disk inclination, the literature values of v sin i, the mean effective temperature observed (27 000 K), and the V band magnitude (with disk contribution removed, $V_{\rm mag}$ = 2.27) to explore a range of stellar models to indirectly constrain the fundamental properties of the star. We find the star has a likely mass between 14 and 18 $M_{\odot}$, with a major axis uniform disk diameter of 0.48 mas and minor axis uniform disk diameter of 0.40 mas when accounting for rotation and gravity darkening. Since this asymmetry is not observable with our current angular resolution, we have adopted a mean diameter 0.44 mas for the modeling work here. Our result is consistent with literature estimates of 0.45 mas diameter (e.g., Stee et al. 1998).

In the near-IR band (1.65 μm) the two models give similar reduced χ^2, i.e. about 4. With our dataset, we cannot neither confirm nor rule out the existence of a cavity between the stellar surface and the circumstellar disk. We note that the parameters of a ring are clearly less constrained than those of a Gaussian disk. However, the extension ($\theta_{\rm disk}$), flattening, and PA are roughly compatible for the two models. Using a stellar diameter of 0.44 mas the measured major axis, i.e. 0.82 for the Gaussian model, corresponds to about 1.9 $D_{\star}$. Assuming that the disk is geometrically thin we can deduce from the measured flattening f an inclination angle of $i = 41 \pm 4°$.

The χ^2 of the models improves substantially if one fits the individual epochs separately rather than combining them all together. This suggests some temporal variability, which is reasonable over periods of a month or two. In Table 3 we have used the variation of the disk parameters as a proxy for our parameter uncertainties, instead of the formal error from LITPRO. Another possible source of error is that we have neglected to account for the known companion in the system. We have searched for a companion during the individual epochs and find no obvious stellar companion for $f_{\rm companion} > 2\%$ (of total H band flux), roughly limiting the spectral type of the companion to be later than F5 ($M_{\rm companion} \sim 1.4\ M_{\odot}$.)

We have also used the LITpro software to fit the VEGA data in the Hα nearby continuum (Visible band, referred to as "R" band in Paper I). We were only able to obtain a good fit of

Table 3. Best parameters obtained with `LITpro` for γ Cas visible and near-IR band data.

Parameters	Gaussian model		Ring model
	Visible band	near-IR band	near-IR band
$\theta_{\rm disk}$ (mas)	0.76 ± 0.05	0.82 ± 0.08	0.85 ± 0.45
$\delta\theta_{\rm disk}$ (mas)	–	–	0.25 ± 0.26
f	1.36 ± 0.08	1.33 ± 0.08	1.39 ± 0.08
PA (deg)	19 ± 5	12 ± 9	12 ± 9
$F_{\rm disk}$ (%)	45 ± 9	53 ± 2	41 ± 6
$F_{\rm bg}$ (%)	–	12 ± 1	14 ± 1
χ^2_r	3.03	3.96	3.95

Notes. $\theta_{\rm disk}$ is the FWHM of the major axis of the Gaussian distribution, $\delta\theta_{\rm disk}$) the ring width, $F_{\rm disk}$ the relative environment continuum flux, f the flattening ratio of the major to the minor Gaussian distribution axis, and PA the position angle of the major axis of the disk measured eastward from the north.

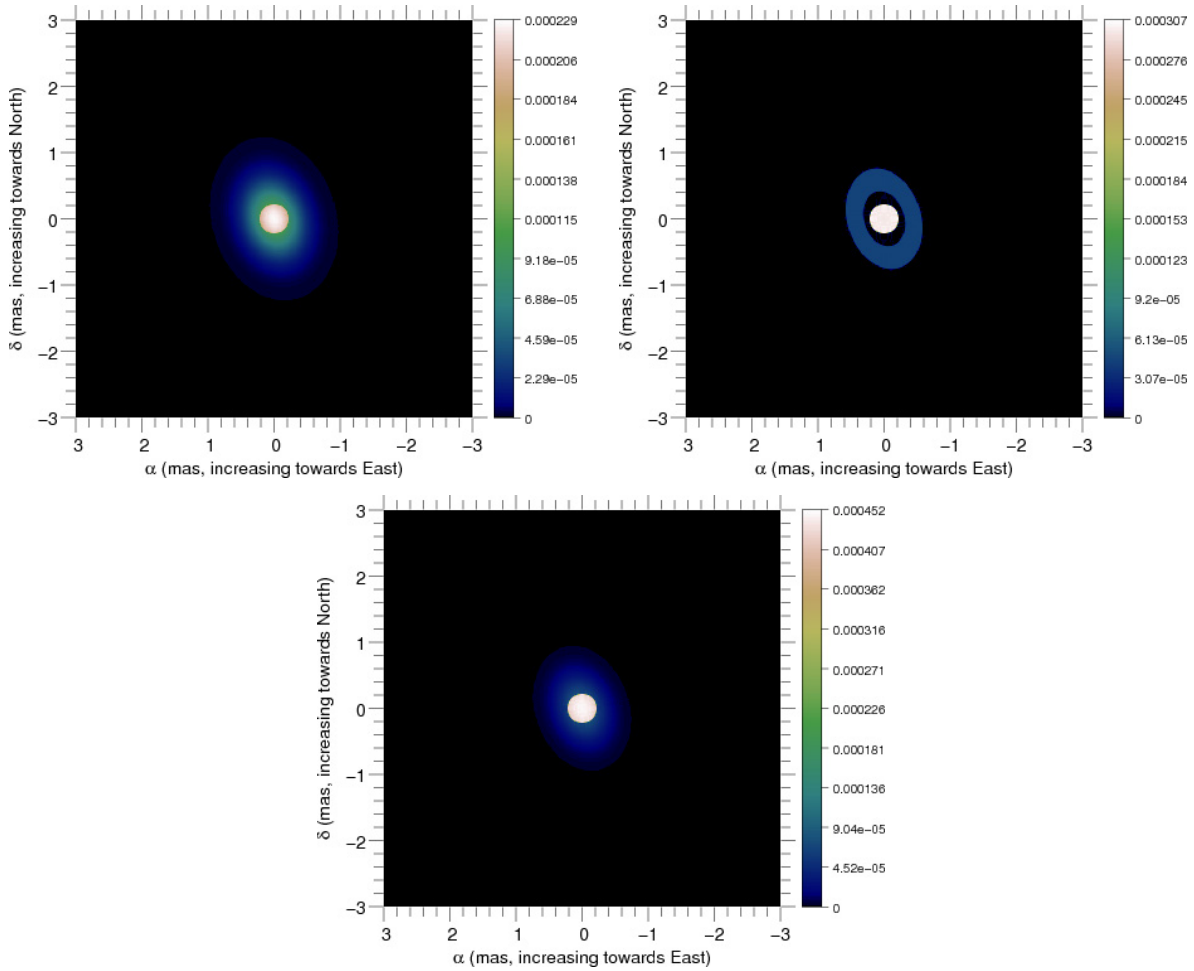

Fig. 4. *Upper left.* LITpro model of γ Cas disk in the H band assuming a uniform central star with a surrounding Gaussian disk and a uniform background. *Upper right.* LITpro model of γ Cas disk in the H band assuming a uniform central star with a surrounding ring and a uniform background. *Lower-central.* LITpro model of γ Cas disk in the nearby continuum of the Hα emission line assuming a uniform central star with a surrounding Gaussian disk.

the data with a Gaussian model. For this model we found that the disk is smaller (though within the errors) in the Visible band continuum than in the near-IR band, i.e. $\theta_{\rm disk} = 0.76 \pm 0.05$ mas vs. 0.82 ± 0.08. This corresponds to a disk major axis of 1.7 $D_\star$. The flattening ratio is similar to that determined in the near-IR band from the MIRC data, i.e. $f = 1.36 \pm 0.08$, and assuming again a geometrically thin disk it corresponds to an inclination angle $i = 42 \pm 4°$. We also tried to fit the data with a ring model, but the χ^2_r obtained were always larger than for the Gaussian model, e.g. $\chi^2_r > 4.2$ to be compared with $\chi^2_r = 3.03$ for a disk in contact with the stellar photosphere. Moreover, the solutions obtained with a ring model were all converging to an inner ring diameter equal to the stellar diameter, i.e. a solution in contact with the stellar surface. Finally, we also note that the stellar contribution to the total flux decreases between the visible and near-IR band from 55 to 25%.

We must emphasize that the addition of a uniform background, which is supposed to mimic a possible disk contribution from previous mass loss or from a more diluted and extended disk, has merely improved the reduced χ^2. It has not changed our previous results regarding the disk sizes with an extended elliptical Gaussian distribution or a flattened ring. We also want to mention that a ring scenario may not be physically consistent as argued by Carciofi et al. (2012). In our models we did not include important effects from radiative and viscous processes in the disk. Carciofi et al. (2012) have shown that a gap between the star and the inner disk is not a stable configuration. Even if mass injection from the Be star ceases, turbulent viscosity can be expected to rearrange disk matter and fill an inner gap. However, this argument holds only in the absence of magnetic fields. As argued by Paper I and work cited therein, there is considerable indirect evidence for disorganized fields emerging from the surface of the Be star. Therefore, it is premature to predict whether the disk extends to the star or not in this complicated environment. However, we do not expect magnetic effects to be important beyond about 1 R_* above the surface. This is relevant because for other Be stars at least Carciofi (2012) places the H-band continuum formation region at 1−2 R_*. This is consistent with our fit of the Gaussian disk *FWHM* of 0.82 mas. For the flattened ring model, in which a larger inner gap is assumed, the fitted inner gap is about 0.60 mas and the ring radius 0.85 mas.

6. Kinematics of the circumstellar envelope

Figures 5 and 8 display the differential visibility modulus (also known simply as visibility) and phase as a function of wavelength around the Hα line obtained by cross-spectral processing with the parameters of Table 1. The visibility curves clearly

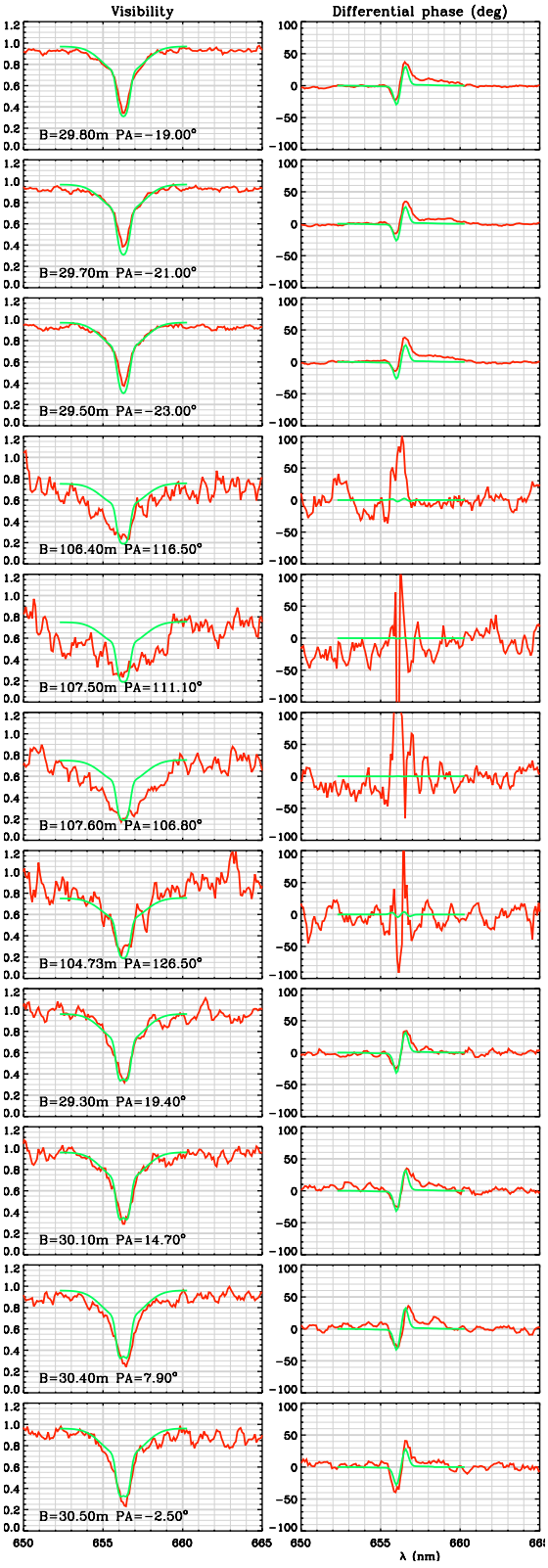

Fig. 5. γ Cas calibrated medium spectral resolution (5000) measurements: visibility (*left*) and differential phase (*right*) for different baseline length and PA indicated on each plot. The visibility and phase from our best-fit model is overplotted in green (plain line).

indicate that the Hα region is partially resolved with the smallest baselines and fully resolved with the largest baselines. We also notice the presence of a large broadening in the wings of the visibility curves. Regarding the differential phase plots, we see that they exhibit "S" shapes, which are clear signatures for rotating disks (Meilland 2007a, 2012). Finally, let us note the complex behavior of the differential phase for the largest baselines. It is mainly due to the fact that the disk is fully resolved, which implies that there is no longer a direct relation between the photocenter displacement and the fringe pattern shift (a first order effect observed when the object is unresolved or barely resolved). Observations are then rather sensitive to small scale features in the disk, which are neither taken into account nor reproduced by the simple kinematic disk-model that we present in the next section.

6.1. The kinematic model

To constrain the kinematics of the circumstellar environment, we used a simple model developed for fast fitting of spectrally-resolved observations of rotating and/or expanding geometrically thin disks around stars. This model is described in detail in Delaa et al. (2011) and was already used to interpret several spectro-interferometric observations of Be stars (Meilland et al. 2011, 2012), and B[e] stars (Millour et al. 2011).

Previous work on kinematics of Be star circumstellar environments using spectroscopy (Miroshnichenko et al. 2003; Kanaan et al. 2006) and spectro-interferometry (Meilland et al. 2007a,b, 2011, 2012; Carciofi et al. 2009; Kraus et al. 2011) has shown that the disk kinematics is dominated by rotation and that expansion velocities are on the order of a few km s^{-1} or even smaller. We therefore decided to model the γ Cas disk environment as a purely rotating disk with a velocity field given by a simple power law:

$$V_\phi = V_{\rm rot}\left(\frac{r}{R_\star}\right)^\beta \quad (1)$$

where $V_{\rm rot}$ is the rotational velocity at the inner rim of the disk and r is the distance to the center of the star. If the disk is directly connected to the photosphere and no acceleration or deceleration layer exists between the two, then $V_{\rm rot}$ is the stellar rotational velocity. Moreover, if the disk is in Keplerian motion, $V_{\rm rot}$ should be equal to the critical velocity ($V_{\rm c}$) and $\beta = -0.5$.

The model parameters can be classified into 4 categories:

1. The stellar parameters: stellar radius ($R_\star$), distance (d), inclination angle (i), and disk major-axis position angle (PA).
2. The kinematic parameters: rotational velocity ($V_{\rm rot}$) at the disk inner radius (i.e., photosphere) and exponents of the rotational (β) velocity law.
3. The disk continuum parameters: disk FWHM in the continuum ($a_{\rm c}$), disk continuum flux normalized by the total continuum flux ($F_{\rm c}$).
4. The disk emission line parameters: disk FWHM in the line ($a_{\rm H\alpha}$) and line equivalent width (EW$_{\rm H\alpha}$).

Delaa et al. (2011) showed that the Hα line profiles were often affected by non-kinematic broadening due to non-coherent scattering, and we used their simple ad hoc method to take this into account. Thus, two additional parameters are introduced in our simple kinematic-model: the global ratio of the scattered photons (R) and the spectral width of the scattering (W).

Finally, our simple model enables us to calculate a 256 × 256×100 data-cube corresponding to 256×256 pixels of the map and 100 different wavelengths in the line and nearby continuum in less than one second on a "standard" computer. The wavelength dependent visibilities and phases for several baselines can

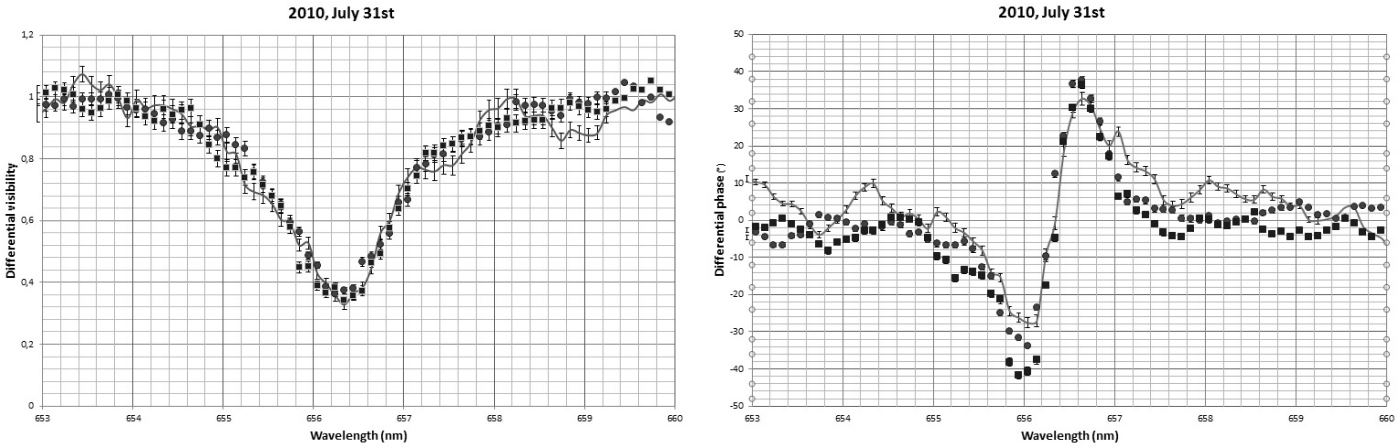

Fig. 6. Differential visibilities (*left*) and phases (*right*) obtained on γ Cas in natural light (lines), for the linear polarization denoted H (squares) and for the linear perpendicular polarization denoted B (circles) on 2010 July 31.

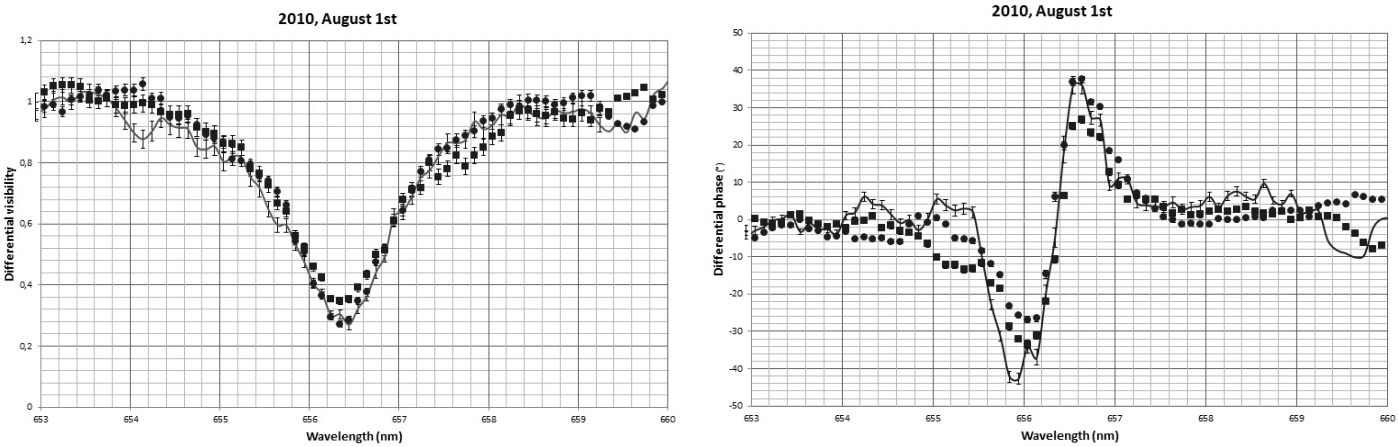

Fig. 7. Differential visibilities (*left*) and phases (*right*) obtained on γ Cas in natural light (lines), for the linear polarization denoted H (squares) and for the linear perpendicular polarization denoted B (circles) on 2010, August, 1st.

finally be calculated with Fourier transform methods. The total computing time for one simulated interferometric dataset is on the order of a few seconds.

6.2. Results

We fixed some of the model free-parameters to previously determined values. The distance 168 ± 20 pc is estimated from van Leeuwen (2007) revised Hipparcos parallaxes, the major axis position angle and the inclination angle are derived from the fit of the *H* band continuum data, and the stellar radius is set to 10 $R_\odot$. The best-fit model parameters are presented in Table 4 and the modeled visibilities and differential phases are over-plotted in Figs. 5 and 8. From Fig. 5 we see that the agreement with our simple model is not very good, especially in the line wings, for two reasons: first, using the medium (5000) spectral resolution we have few measurements across the visibility modulus and phase and, second, our simple model is not accurate enough to mimic the complex visibility behavior for the largest baselines which are sensitive to fine structure within the disk. On the other hand, we can see from Fig. 8 that the agreement is better for the HR (30 000) data first because the number of measurements is larger across the visibilities and phases and second because these measurements correspond to small projected baselines (~30 m) which are more sensitive to the global disk geometry rather than small spatial structure. The global reduced χ^2 of the best-fit model is 3.1 with a better χ^2 of 1.6 for the HR data and a lower poorer value of 7.6 for the MR data.

We must mention that our simple modeling predicts "double-peak" visibility profiles. This is apparent in each profile with a "W" shape of Fig. 8. As discussed by Meilland et al. (2007a, 2012), these W features are often seen in the observed LBOI data for Be stars. The absence of this feature here means that γ Cas appears larger at the center of the emission line compared to its size in the nearby emission line wings. This is contrary to what was found for instance for α Arae by Meilland et al. (2007) and might be related to the fact that opacity effects such as scattering are certainly important in the disk of γ Cas and are not taken into account here. We also note that we could not model the data correctly without assuming that most of the Hα emission line is strongly affected by Thomson and non-coherent scattering out to a few hundred km s^{-1} as already outlined in Delaa et al. (2011). Our procedure was to select as additional fitting parameters a flux fraction R smeared by a wavelength Gaussian parameter W in Å. As Table 4 shows, our best fit was achieved with a fraction R = 50% and a Gaussian *FWHM* of 25 Å. The wings in our spectral profiles (see Fig. 2) are clearly more extended than in

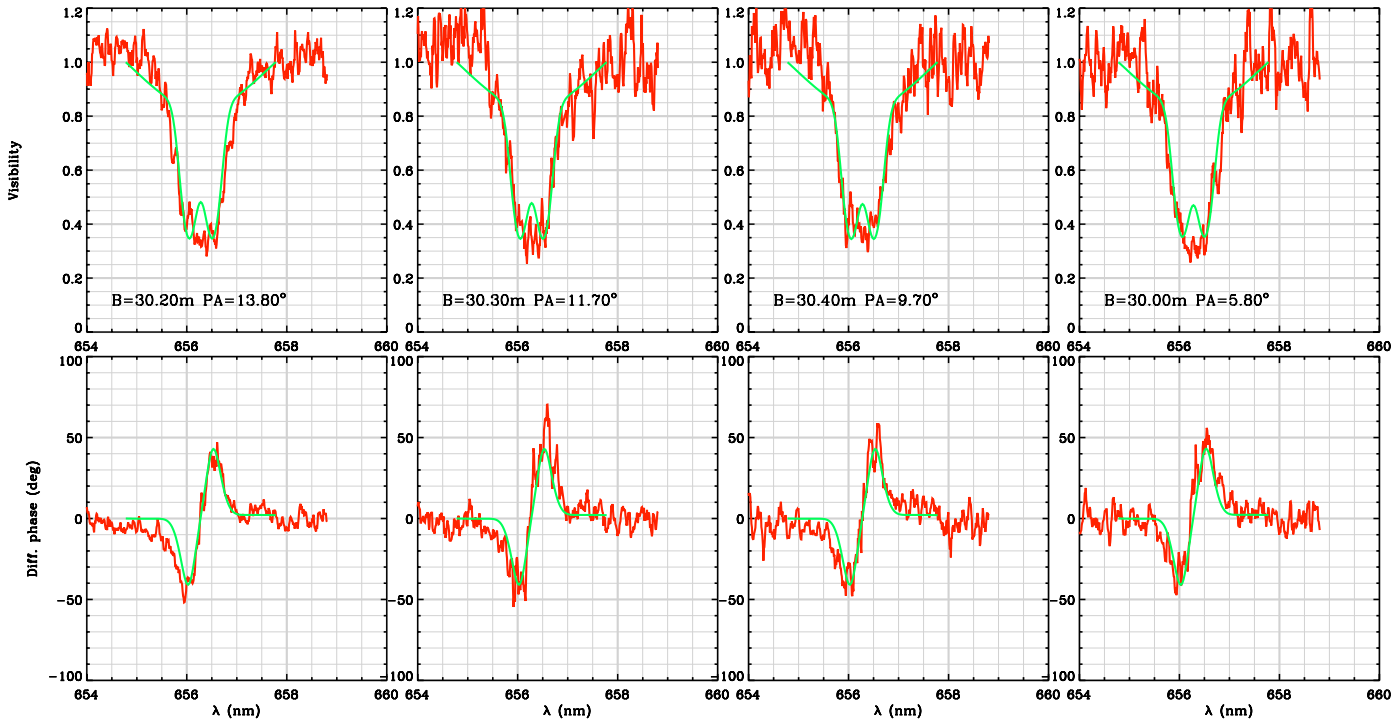

Fig. 8. γ Cas calibrated high spectral resolution (30 000) measurements: visibility (*top*) and differential phase (*bottom*) for different baseline lengths and PA indicated on each plot. The visibility and phase from our best-fit model is overplotted in green (plain line).

Table 4. Values of the best-fit kinematic model parameters.

Parameter	Value	Remarks
	Global geometric parameters	
$D_\star$	10.0 $D_\odot$	≃0.44 mas
d	168 pc	from von Leeuween (2007)
i	42°	from visible and near-IR bands data fit
PA	$20 \pm 15°$	
	Global kinematic parameters	
$V_{\rm rot}$	550 ± 50 km s^{-1}	$\approx V_c$
β	0.5 ± 0.1	Keplerian rotation
	Hα disk geometry	
$a_{\rm H\alpha}$	10.0 ± 1.0 $D_\star$	$=4.4 \pm 0.4$ mas
$EW_{\rm H\alpha}$	28.0 ± 3.0 Å	
	non-coherent scattering	
R	50 ± 20 %	
W	25 ± 10 Å	

the BeSS data, but one cannot ignore the large diffusion effect generating these extended wings seen in both data sets. Thus the interpretation of the R and W parameters introduced to reproduce these large wings is not straightforward and may not be entirely linked to the physics within the circumstellar disk.

6.3. Differential visibilities in polarized light

The natural and polarized light visibility curves are similar (Figs. 6 and 7 left) and can be reproduced by our model (see lower panels of Fig. 5) – no significant changes of the characteristic size in the Hα line are observed with polarization.

Differential phase curves in polarized light (Figs. 6 and 7 right), show differences in amplitude and in shape. The differences between natural and polarized light are always larger than the variance of the measurements. Moreover we have checked that observations of an interferometric calibrator show phase curves which are flat with wavelength and do not present such differences between natural and polarized light.

As an example, the S-shape on γ Cas is deeper in the blue wing for the polarized H than for the natural light on July 31 whereas the trend is reversed on 1 August. Since polarization signals are a tracer of asymmetry and as our interferometric observations favor the analysis along two orientations on the sky, these differences by date may be related to the different orientation of the Wollaston prism on the sky: the VEGA spectrograph slit (and thus the Wollaston prism) orientation depends upon the hour angle and the target coordinates. The PA of the slit equals −10° on July, 31 and −25° on August, 1 to be compared with the PA of the disk (+19±5°). The measured differences between July and August cannot reasonably be interpreted by an intrinsic time dependence of the polarization of the source since polarimetric monitoring of γ Cas over one year by Harrington & Kuhn (2009) found only a change of 0.3% of the measured polarization. For the moment our model is not designed to reproduce these effects and new developments will be needed for interpreting such spectro-polarimetric interferometric measurements.

7. Discussion

7.1. New results for the disk geometry

By exploiting the capabilities of the VEGA instrument we were able to measure the disk extension in the nearby Hα continuum, i.e. 0.76 and 0.56 mas respectively, for the major and minor axes,

assuming a Gaussian envelope. This is perfectly consistent with the previous measurement of 0.78 mas by Stee et al. (1998) assuming a circular geometry using the GI2T interferometer with its north-south baseline. Moreover, the poor (u, v) plane coverage and the small baseline of the GI2T interferometer were not sufficient to measure any flattening and PA of the envelope in the nearby Hα continuum which is not the case with our VEGA data. In the Hα line, the VEGA resolution allows us to select spectral channels coming from a portion of the emission line *only*. We detect a flattened envelope with an extension of 4.4 mas, i.e., $10 \pm 1\ D_*$ using a central stellar disk diameter of 0.44 mas, again consistent with the measurement of 4.05 mas or $9\ D_*$ by Stee et al. (1998). This extension of 4.4 ± 0.4 mas is larger than obtained by Quirrenbach et al. (1997) and Tycner et al. (2003). With our star angular diameter of 0.44 mas their results become $7.9\ D_*$ and $8.3\ D_*$ respectively. We believe the primary reason for these smaller disk extensions is that the former measures were made in filtered bandpasses (up to 100 Å), for which the contribution of the (less resolved) continuum flux is much more important. Our high resolution results are less contaminated by the continuum flux and thus lead to a truer representation of the Hα emitting disk area. Finally, this is the first direct evidence that the disk has grown in size between 1997 (Tycner's measurements) and 2010 (our measurements) as suggested by the strengthening of the Hα emission, e.g. Fig. 1 of Paper I, even if this is at a 1σ level of confidence.

In the near-IR band at 1.65 μm, the MIRC data are consistent with a Gaussian disk or a ring model with a similar reduced χ^2. Assuming a Gaussian envelope we obtain a disk major axis of 0.82 mas and a minor axis of 0.62 mas. In the nearby Hα continuum the major and minor axes are smaller than in the near-IR band as predicted by Touhami et al. (2011).

Assuming a geometrically thin circular disk, the disk flattening in the near-IR and Visible data in the continuum, i.e. 1.33 and 1.36, are in very good agreement and correspond to an inclination angle of ~42°. The latter value was used as an input parameter for the kinematic model. The PA of $19° \pm 5$ from the VEGA data in the continuum is also in very good agreement with the same value obtained by Quirrenbach et al. (1997) and consistent with the $12° \pm 9$ estimated from MIRC measurements at 1.65 μm. Note that the PA of $20° \pm 15$ obtained with the kinematic model, even if consistent with the other values, is poorly constrained due to the fact that γ Cas is fully resolved with the largest baselines. McDavid (1999) found an intrinsic polarization angle that corresponds to a PA = 20°.

Using long-term visual spectrophotometric data of Be stars (including γ Cas), Moujtahid et al. (1999) found that the electron density in the circumstellar envelope of Be stars should never exceed 10^{13} cm^{-3} and that the radii of regions producing the spectro-photometric variations do not exceed 2–10 R_*. Their data do not support strongly flattened circumstellar envelopes since in that case, it is not possible to produce the amount of emission currently observed in the V band without violating the circumstellar envelope density limitations imposed by the characteristics of the second component of the Balmer discontinuity. Our simple geometric and kinematic models are assuming a very thin disk but our interferometric measurements cannot rule out less flattened circumstellar envelopes. The small envelope of 1.86 and 1.72 R_* respectively in the near-IR and visible continuum spectral bands is certainly the region where these spectrophotometric variations originate (i.e. within the denser part of the disk) and also corresponds to the region where Berio et al. (1999) found the one-armed structure.

7.2. The binarity of γ Cas

The question of an unseen companion orbiting around γ Cas becomes an issue when studying the origin of its hard X-ray flux, if indeed the X-rays are formed from infall from Be efflux onto the potential well of a degenerate companion (e.g., White et al. 1982). Harmanec et al. (2000) have in fact found that γ Cas is a binary by analyzing radial velocities (RV) from 295 Reticon spectrograms obtained between 1993 October and 2000 May. They found that γ Cas is the primary component of a spectroscopic binary with a period of 203.59 d and an eccentricity of 0.26. The mass of the secondary is about 1 $M_\odot$.

In a follow up radial velocity study of the system, Miroshnichenko et al. (2002) reached the same conclusion, Analyzing high resolution observations of the Hα line obtained at Ritter Observatory between 1992 and 2002, these authors found a slightly different period of 205.5 days, with a circular orbit. In the past year the discrepancy between the eccentricities in these two orbital solutions has been resolved in favor of near-circularity by two new papers. Nemravová et al. (2012) found a period of 203.52 ± 0.08 days and an immeasurably small eccentricity e. In Paper I we analyzed a separate set of velocities in addition to the Ritter RVs and found a practically equivalent result, $P = 203.5 \pm 0.2$ days with $e < 0.03$. The secondary star's mass is $0.9 \pm 0.4\ M_\odot$, where the error bars are probably generous.

As a further constraint, we have no evidence of binarity from our interferometric measurements, neither a modulation of the visibility modulus as a function of time or spatial frequency, nor a phase modulation of the fringes. This is not surprising because the difference of magnitude in the visible between the primary and the secondary is certainly too large, i.e. $\delta m_V > 3$, even if the angular separation of the 2 components between 8 and 10 mas is well suited for the interferometer field of view. This non-detection reinforces the fact that the secondary is certainly a low-mass and low-luminosity star or a degenerate companion with a much lower luminosity than the primary as already outlined by Harmanec et al. (2000). Nevertheless, we have tested this binary hypothesis with various models, using the LITpro software, assuming a central star + a Gaussian disk with the parameters in Table 3 and a stellar companion supposed to be unresolved. We obtain only a slightly better χ^2 of 1.83 compared to 1.9 for a 4.2 mag fainter companion located at ~0.5–0.7 mas from the central star, i.e. within the circumstellar disk. This is not a physically acceptable solution and is not compatible with the orbital parameters determined by Harmanec et al. (2000), i.e. a companion at a distance larger than 7 mas.

However, binarity may be indirectly detected as it influences the circumstellar environment geometry. In the case of δ Sco (Meilland et al. 2011), a companion with an eccentric orbit coming close at periastron may trigger disk formation triggered by tidal effects even if the star is rotating below its critical velocity. Such a mechanism is also suspected for Achernar (Kervella et al. 2007). For α Arae a putative companion was also detected by Chesneau et al. (2005), but if its orbit is more circular the disk may be permanent and confined within the Roche lobe of the system. We note that we also found for γ Cas that the disk radius in the Hα line would be about half the Roche lobe radius ($21.4\ R_*$) of a binary system (Gies et al. 2007; Touhami et al. 2011) even if we see no evidence for binarity in our visible interferometric data. We find from Okazaki & Negueruela (2001) that the most likely 3:1 resonance truncation radius of the disk due to the companion is about 0.4 of the orbital separation, or $\sim\frac{3}{4}$ of the Roche lobe radius. Our VEGA radius does not yet reach this extent, but one may hope more sensitive future observations

could test for the presence of a truncation edge. However, truncation efficiency also depends on orbital size and may not be very strong in the case of γ Cas (Okazaki 2009, priv. comm.).

Note that binarity may also be a way to explain the near critical rotation of γ Cas, as is certainly the case for the well known binary system ϕ Per where the Be star is rotating critically because it has been spun up by its companion (Gies et al. 1998). Thus, in a possible scenario γ Cas may have have been spun up by previous mass transfer from a now degenerate companion, which is not necessarily accreting.

7.3. Circumstellar kinematics: Keplerian rotation

Before our observations, the question of the velocity law in the equatorial disk of γ Cas was still an open issue, even if Mourard et al. (1989) had already detected disk rotation. In the study of the rotational component of the wind in the γ Cas envelope, Stee (1996) found that constant and solid body rotation laws can be rejected. Nevertheless, following the variation of the photocenter displacement into the sky plane they were not able to distinguish between a momentum conservation ($\beta = 1.0$), a Keplerian ($\beta = 0.5$) and a $\beta = 0.25$ circular velocity law.

The infrared spectrum of γ Cas was observed by Hony et al. (2000) with the ISO-SWS instrument between 2.4 and 45 μm. They found that the line strengths of hydrogen Brackett series lines indicate that the lines are optically thick and formed at high densities in the inner disk with a temperature above the bulk of the disk material. Moreover, the FWHMs of the weakest series members, formed closest to the star, suggest they are rotating in excess of 550 km s^{-1}. This is similar to the photospheric equatorial rate, taking into account the gravity darkening, and suggests the presence of emission very close to the stellar photosphere. In our opinion, we do not need to advocate for solid-body rotation as proposed by Hony et al. (2000), since from our kinematical analysis in Sect. 6 we obtained exactly the same velocity within the disk but with direct evidence for a globally Keplerian disk compared to a solid-body rotation law. Note that this is true for the disk as a whole since we cannot distinguish β for a small portion of it.

It has been confirmed that γ Cas is rotating close to its critical velocity, which was estimated to be $V_{\rm eq} = 577 \pm 36$ km s^{-1} by Frémat et al. (2005). The first argument comes from the star's $v \sin i$ and the i we have redetermined as near $i = 42°$. An additional argument for γ Cas rotating near criticality comes from the observation of a robust feature in the star's light curve with a period of about 1.21581 days. This period is in good agreement with expectation for a critical rotation rate based on the star's estimated radius and the inclination (Smith et al. 2006).

7.4. Is critical rotation necessary for the Be phenomenon?

Be stars are known to be fast rotators. However, their rotational rate is still highly debated. For instance, Frémat et al. (2005) determined a mean rotational rate of $\Omega/\Omega_{\rm c} = 0.88$ by modeling photospheric lines of 130 Be stars using the NLTE code FASTROT. On the other hand, in a statistical study of the $v \sin i$ of 462 Be stars, Cranmer (2005) found that some of the hottest Be stars ($T_{\rm eff} > 18\,000$ K) may rotate down to 50% of their critical velocity whereas some later Be stars seem to be critical rotators. After the first VLTI/AMBER spectro-interferometric observations of Be stars (Meilland et al. 2007a,b), Stee & Meilland (2009) proposed the hypothesis that classical Be stars may not be an homogeneous group in term of processes responsible for the mass-ejection.

A first subgroup may be composed of nearly critically rotating stars. This nearly critical rotation, even if not sufficient by itself to initiate the mass loss, might be the dominant physical process responsible for the equatorial disk formation by drastically reducing the local gravity. Smaller effects from non-radial pulsations as proposed by Osaki (1986), viscosity drifting (Lee et al. 1991), magnetism (Yudin et al. 2010), or binarity (Harmanec et al. 2002) may explain the compensation of the remaining effective gravity.

The second subgroup of Be stars may be composed of objects rotating below 80% of their critical velocity. In this case the rotation itself cannot compensate for more than half the effective gravity at the equator. Another physical process or combination of processes probably dominate the ejection of matter. Such a physical process could be non-radial pulsations as proposed by Cranmer (2005) or binarity in some cases (for example see δ Sco's study using interferometry by Meilland et al. 2011). A significant direct effect from radiative pressure can be ruled out as it would produce an equatorial wind (Lamers et al. 1991) with an expansion velocity of more than 10 km s^{-1} which is not in agreement with observations (see for example Miroshnichenko et al. 2003; Kanaan et al. 2008).

In any case it is clear that disks cannot be formed from radiative and rotational processes alone, but rather need help from at least one ill understood mechanism, a "deus ex machina". To quantify the problem of disk maintenance in a "typical" classical Be star, Carciofi et al. (2012) have found that mass loss rates an order of magnitude higher than expected from a radiative wind are required to maintain a disk for 28 CMa. Whatever the mechanism, it must be triggered by an instability in order to explain the episodic nature of disk ejection "episodes". This difficulty is much the same for γ Cas and its X-ray emitting analogs. However, as noted in Sect. 2, correlated optical/X-ray variations of γ Cas suggest that circumstellar matter mediates the level of X-ray flux we observe and therefore seems to be an essential ingredient in generating hard X-ray emission.

In the first spectro-interferometric survey of 8 Be stars, Meilland et al. (2012) found a mean rotational rate of $\Omega/\Omega_{\rm c} = 0.95 \pm 0.02$, very close to critical rotation, and no dependence on their effective temperatures. Their current sample is probably too small to conclude on this second point. Nevertheless, such a high rotational rate favors the hypothesis that rotation is the dominant phenomenon in the mass-ejection process for many Be stars.

Under this simple scheme and assuming an inclination angle of 42°, $v \sin i = 441 \pm 27$ km s^{-1} and a $V_{\rm c} = 577 \pm 36$ km s^{-1} (Frémat et al. 2005), γ Cas would support the Meilland et al. (2012) conclusion that Be stars rotate close to their critical velocity (i.e. $V_{\rm rot}/V_{\rm c} = 1.15 \pm 0.15$).

The main issue in all these attempts to determine the Be star rotational rates (i.e. $V_{\rm rot}/V_{\rm c}$) is the impact of several uncertainties: the stellar mass, the stellar radius, and the inclination angle. Moreover, the effect of rotation on the stellar flattening and effective temperature may also introduce additional biases. Finally, a statistical study combining high spectral and spatial resolution on many lines and on a large sample (at least 50 objects) and/or the discovery of a critically rotating star in an edge-on eclipsing binary system, may help to solve this issue.

8. Conclusion

Thanks to these first spectrally resolved observations combined with a multi-technique, multi-site observing campaign,

including Automated Photometric Telescope (APT) measurements, *XMM-Newton* observations and Hα spectroscopic follow-up presented in Paper I, we can conclude the following:

- CHARA observations have enabled modeling of the γ Cas disk in two different wavelength regimes as well as Hα line flux. The measured inclination of the Be disk relative to our line of sight is consistent with previous observations. In all cases the observations have pushed the size of the disk to greater proportions.
- The VEGA kinematic measurements show decisively that the disk rotation relation is consistent with Keplerian rotation. This seems to be a general tendency since 10 Be stars already studied have a Keplerian circumstellar disk (Meilland et al. 2007a; Stee & Meilland 2009; Delaa et al. 2011; Meilland et al. 2011; 2012). Note that Keplerian rotation was already supported, even if indirectly, by spectroscopic measurements almost a decade earlier by Rivinius et al. (1999, 2006). γ Cas has been confirmed to be a nearly critical rotator and critical rotation seems to play a major role in the Be phenomenon. Solid body rotation is therefore ruled out for the whole disk. The confluence of Keplerian rotation with solid body rotation of corotating clouds over the stars surface advocated in Paper I suggests a more complicated geometry for the circumstellar matter.
- The disk seems to be in contact with the central star in the near infrared and in the visible continuum, even if a "ring" geometry cannot be ruled out from our near infrared observations. Nevertheless, even for this ring geometry, the gap between the stellar surface and the inner part of the disk appears to be small and the picture of a stellar corotating magnetosphere between 3 to 7 $R_\star$ as usually advocated for T Tauri stars (Getman et al. 2008) seems applicable to γ Cas. Note that it does not mean that γ Cas has no magnetosphere at all but if this is the case, it does not extend out to 3 $R_\star$.
- The disk imaging gives no indication of a 1-arm spiral feature. This is consistent with the absence of *V*, *R* emission features in the Hα line profile. Evidently, the 1-arm feature disappeared shortly before 2000 (as noted in Paper I).
- The LBOI imaging gives no indication of a secondary star. This non-detection supports the interpretation that the secondary is certainly a low-mass and low-luminosity star or a degenerate companion with a much lower luminosity than the primary as already outlined by Harmanec et al. (2000).

Acknowledgements. J.D.M. would like to acknowledge support from the University of Michigan for funding the original construction of MIRC and NSF-AST 0707927 which funded the observations of γ Cas. R.L.O. acknowledges financial support from the Brazilian agency CNPq (*Conselho Nacional de Desenvolvimento Científico e Tecnológico*) through Universal 14/2011 Grant 470361/2011. The CHARA/VEGA project has benefited from funding from the French Centre National de la Recherche Scientifique (CNRS) through the Institut National des Sciences de l'Univers (INSU) and its Programmes Nationaux (ASHRA, PNPS). S.T.R. acknowledges partial support from NASA grant NNH09AK731. This work has made use of the BeSS database, operated at GEPI, Observatoire de Meudon, France: http://basebe.obspm.fr.

References

Abbott, D. C. 1979, IAUS, 83, 237A
Apparao, K. M. V., & Tarafdar, S. P. 1997a, J. Astrophy. Astron., 18, 145
Apparao, K. M. V., & Tarafdar, S. P. 1997b, BASI, 35, 345
Ashok, N. M., Bhatt, H. C., Kulkarni, P. V., et al. 1984, MNRAS, 211, 471
Berio, Ph., Stee, Ph., Vakili, F., et al. 1999, A&A, 354, 203
Blouin, D., McCutcheon, W. H., Dewdney, P. E., et al. 1997, MNRAS, 287, 455
Carciofi, A. C., Domiciano de Souza, A., Magalhaes, A. M., et al. 2008, ApJ, 676, L41
Carciofi, A. C., Bjorkman, J. E., Otero, S. A., et al. 2012, ApJ, 744, 15
Cranmer, S. R. 2005, ApJ, 634, 585
Che, X., Monnier, J. D., & Webster, S. 2010, Proc. SPIE, 7734, 77342
Che, X., Monnier, J. D., Zhao, M., et al. 2011. ApJ, 732, 68
Chesneau, O., Meilland, A., Rivinius, T., et al. 2005, A&A, 435, 275
Coté, J., & Waters L. B. F. M. 1987, A&A, 176, 93
Domiciano de Souza, A., Kervella, P., Jankov, S., et al. 2003, A&A, 407, L47
Dougherty, S. M., & Taylor, A. R. 1992, Nature, 359, 808
Frémat Y., Zorec J., Hubert A.-M., et al. 2005, A&A, 440, 305
Gehrz, R., Hackwell, J., & Jones, T. 1974, ApJ, 191, 675
Getman, K. V., Feigelson, E. D., Micela, G., et al. 2008, ApJ, 688, 437
Gies, D. R., Bagnuolo, W. G. Jr, & Ferrara, E. C. 1998, ApJ, 493, 440
Gies, D. R., Bagnuolo, W. G. Jr, Baines, E. K., et al. 2007, ApJ, 654, 527
Grundstrom, E. D., & Gies, D. R. 2006, ApJ, 651, L53
Güdel, M., & Nazé, Y. 2009, A&ARv, 17, 309
Harmanec, P., Habuda, P., Stefl, S. N., et al. 2000, A&A, 364, L85
Harmanec, P., Bisikalo, D. V., Boyarchuk, A. A., et al. 2002, A&A, 396, 937
Harrington, D. M., & Kuhn, J. R. 2009, ApJS, 180, 138
Henrichs, H. F., Hammerschlag-Hensberge, & Howarth, I. D. 1983, ApJ, 268, 807 (HHH)
Henry, G. W., & Smith, M. A. 2012, ApJ, submitted
Hony, S., Waters, L. B., & Zaal, P. A. 2000, A&A, 355, 187
Horaguchi, T., Kogure, T., Hirata, R., et al. 1994, PASJ, 46, 9
Howarth, I. D., & Prinja, R. K. 1989, ApJS, 69, 527
Huberl, F. 1995, A&A, 296, 685
Hummel, W. 1998, A&A, 330, 243
Hummel, W., & Vrancken, M. 1995, A&A, 302, 751
Jernigan, J. G. 1976, IAU Circ., 2900
Jones, C. E., Sigut, T. A. A., & Marlborough, J. M. 2004, MNRAS, 352, 841
Kanaan S., Meilland, A., Stee, Ph., et al. 2008, A&A, 486, 785
Kervella, P., & Domiciano de Souza, A. 2006, A&A, 453, 1059
Marlborough, J. M. 1997, A&A, 317, L17
McDavid, D. 1999, PASP, 111, 494
Meilland, A., Stee, Ph., Vannier, M., et al. 2007a, A&A, 464, 59
Meilland, A., Millour, F., Stee, Ph., et al. 2007b, A&A, 464, 73
Meilland, A., Delaa, O., Stee, Ph., et al. 2011, A&A, 532, A80
Meilland, A., Millour, F., Kanaan, S., et al. 2012, A&A, 538, A110
Mennickent, R. E., Sterken, C., & Vogt, N. 1997, A&A, 326, 1167
Millar, C. E., & Marlborough, J. M. 1999a, ApJ, 516, 276
Millar, C. E., & Marlborough, J. M. 1999b, ApJ, 526, 400
Millar, C. E., Sigut, T. A. A., & Marlborough, J. M. 2000, MNRAS, 312, 465
Miroshnichenko, A. S., Bjorkman, K. S., & Krugov, V. D. 2002, PASP, 114, 1226
Monnier, J. D., Berger, J.-P., Millan-Gabet, R., et al. 2004, Proc. SPIE, 5491, 1370
Monnier, J. D., Pedretti, E., Thureau, N., et al. 2006, Proc. SPIE, 6268, 62681
Monnier, J. D., Zhao, M., Pedretti, E., et al. 2007, Science, 317, 342
Motch, C., Lopes de Oliveira, R., Negueruela, I., Haberl, F., & Janot-Pacheco, E. 2007, in Active OB Stars: Laboratories for Stellar & Circumstellar Physics (San Franciso: ASP), 361, 117
Moujtahid, A., Zorec, J., & Hubert, A. M. 1999, A&A, 349, 151
Mourard D., Bosc, I., Labeyrie, A., et al. 1989, Nature, 342, 520
Mourard D., Clausse, J. M., Marcotto, A., et al. 2009, A&A, 508, 1073
Mourard D., Berio, Ph., Perraut, K., et al. 2011, A&A, 531, A110
Nemravová, J., Harmanec, P., Koubský, P., et al. 2012, A&A, 537, A59
Neto, A. D., & de Freitas Pacheco, J. A. 1982, MNRAS, 198, 659
Okazaki, A. T. 1991, PASJ, 43, 75
Okazaki, A. T. 1997, A&A, 318, 548
Okazaki, A. T., & Negueruela, I. 2001, A&A, 377, 161
Osaki, Y. 1986, PASP, 98, 300
Pauls T. A., Young, J. S., Cotton, W. D., et al. 2005, PASP, 117, 1255
Porter, J. M., & Rivinus, T. 2003, PASP, 115, 1153
Prinja, R. K. 1989, MNRAS, 241, 721
Quirrenbach, A., Hummel, C. A., Buscher, D. F., et al. 1993, ApJ, 416, L25
Quirrenbach, A., Bjorkman, K. S., Bjorkman, J. E., et al. 1997, ApJ, 479, 477
Rinehart S. A., Houck, J. R., & Smith, J. D. 1999, AJ, 118, 2974
Rivinius, Th., Stefl, S., & Baade, D. 1999, A&A, 348, 831
Rivinius Th., Stefl, S., & Baade, D. 2006, A&A, 459,137
Robinson, R. D., & Smith, M. A. 2000, ApJ, 540, 474
Robinson, R. D., Smith, M. A., & Henry, G. W. 2002, ApJ, 575, 435
Rousselet-Perraut, K., Vakili, F., Mourard, D., et al. 1997, A&AS, 123, 173
Secchi, A. 1867, Astron. Nachr., 68, 63
Sigut, T. A. A., McGill, M. A., & Jones, C. A. 2009, ApJ, 699, 1973
Smith, M. A., & Robinson, R. D. 1999, ApJ, 516, 866S
Smith, M. A., & Robinson, R. D. 2003, Interplay of Periodic, Cyclic, & Stochastic Variability in Selected Areas of the H-R Diagram, ed. C. Sterken (San Francisco: ASP), 292, 263
Smith, M. A., Robinson, R. D., & Corbet, R. H. D. 1998a, ApJ, 503, 877S
Smith, M. A., Robinson, R. D., & Hatzes, A. P. 1998b, ApJ, 506, 945S
Smith, M. A., Henry, G. W., & Vishniac, E. 2006, ApJ, 647, 1375

Smith, M. A., Lopes de Oliveira, R., Motch, C., et al. 2012, A&A, 540, A53 (Paper I)
Stee, Ph. 1996, A&A, 311, 945
Stee, Ph., 2003, A&A, 403, 1023
Stee, Ph., & Araújo, F. X. 1994, A&A, 292, 221
Stee, Ph., & Meilland, A. 2009, LNP, 765, 195
Stee, Ph., de Araùjo, F. X., Vakili, F., et al. 1995, A&A, 300, 219
Stee, Ph., Vakili, F., Bonneau, D., et al. 1998, A&A, 332, 268
Stothers, R. B., & Chin, C. W. 1995, ApJ, 451, L61
Struve, O. 1931, ApJ, 73, 94
Tallon, I., Tallon, M., Thiébaut, E., et al. 2008, Proc. SPIE, 7013, 44
Taylor, A. R., Waters, L. B. F. M., Bjorkman, K. S., et al. 1990, A&A, 231, 453
Thom, C., Granès, P., & Vakili, F. 1986, A&A, 165, L13
Touhami, Y. Gies, D. R., & Schaeffer, G. H. 2011, ApJ, 729, 17
Townsend, R. H. D., Owocki, S. P., & Howarth, I. D. 2004, MNRAS, 350, 189
Tycner, C., Hajian, A. R., Mozurkewich, D., et al. 2003, AJ, 125, 3378
Tycner, C., Gilbreath, G. C., Zavala, R. T., et al. 2006, AJ, 131, 2710
Tycner, C., Jones, C. E., Sigut, T. A. A., et al. 2008, AJ, 189, 461
Underhill, A. B., Divan, L., Prevot-Burnichon, M.-L., et al. 1979, MNRAS, 189, 601
van Leeuwen, F. 2007, Astrophys. Space Sci. Lib. (Springer), 350
van der Heuvel, E. P. J., & Rappaport, S. A. 1987, in Physics of Be stars, eds. A. Slettebak, & T. P. Snow (Cambridge University Press), IAU Colloq., 98, 291
Vakili F., Mourard D., Stee Ph., et al. 1998, A&A, 335, 261
von Zeipel, H. 1924, MNRAS, 84, 665
Waters, L. B. F. M., Coté, J., & Lamers, H. J. G. L. M. 1987, A&A, 185, 206
White, N. E., Swank, J. H., Holt, S. S., et al. 1982, ApJ, 263, 277
Yudin, R. 2001, A&A, 368, 912
Yudin, R. V., Hubrig, S., & Pogodin, M. A. 2010, IAUS, 272, 224
Zhao, M., Monnier, J. D., Che, X., et al. 2011, PASP, 123, 964